Journal of
Composites Science

MDPI

Article

Polymer Blends and Polymer Nanocomposites for Photovoltaic (PV) Cells and an Investigation of the Material Deposition Techniques in PV Cell Fabrication

George Ntanovasilis, Ioannis Zaverdas, Tarig Ahmed, Foivos Markoulidis and Constantina Lekakou *

Department of Mechanical Engineering Sciences, University of Surrey, Guildford GU2 7XH, UK; g.ntanovasilis@surrey.ac.uk (G.N.); I.Zaverdas@surrey.ac.uk (I.Z.); t.ahmed@surrey.ac.uk (T.A.); f.markoulidis@surrey.ac.uk (F.M.)
* Correspondence: c.lekakou@surrey.ac.uk

Abstract: Polymer photovoltaics (PV) offer the advantage of low-cost, mass-produced, flexible PV films, but they generally suffer from a low-power conversion efficiency (PCE) compared to silicon. This paper studies ITO/PEDOT:PSS/bulk heterojunction/Al PV cells, where two different bulk heterojunction blends are researched: P3HT/PC_{61}BM and PCDTBT/PC_{70}BM. The addition of multiwall carbon nanotubes (CNT) is explored as a conductive network to accelerate the electron transport and extraction to the outer aluminium current collector while reducing the chance of charge recombinations. Several layer deposition techniques are investigated: spin coating and casting, as well as techniques that would induce transverse orientation of polymer grains, including inkjet printing, electrophoresis and the application of a transverse AC field during annealing. Transverse orientation techniques produced architectures that would facilitate charge transport without recombinations, but it is recommended to avoid such techniques for the deposition of conductive PEDOT:PSS and CNT layers as they create a high surface roughness that leads to short circuiting. The best performing PV cell is the ITO/PEDOT:PSS/PCDTBT/PC_{70}BM/CNT/Al structure with a PCE of 11%.

Keywords: carbon nanotubes; semiconductor polymer nanocomposites; semiconductor polymer blends; PEDOT:PSS; inkjet printing; spin coating; casting; photovoltaics

Citation: Ntanovasilis, G.; Zaverdas, I.; Ahmed, T.; Markoulidis, F.; Lekakou, C. Polymer Blends and Polymer Nanocomposites for Photovoltaic (PV) Cells and an Investigation of the Material Deposition Techniques in PV Cell Fabrication. *J. Compos. Sci.* **2021**, *5*, 263. https://doi.org/10.3390/jcs5100263

Academic Editor: Francesco Tornabene

Received: 6 September 2021
Accepted: 28 September 2021
Published: 9 October 2021

1. Introduction

Solar energy is a major renewable energy form, abundant on this planet, and can be harvested by static or moving user applications, including buildings, open spaces, land, air or sea transport vehicles. Crystalline silicon holds about 90% of the photovoltaics (PV) market offering about a 25% energy conversion efficiency [1]. However, there are several issues with this technology, pushing research to 2nd and 3rd generation PV materials: (a) the main material source is special grade silicon, for which there might be a shortage if solar cells are going to be used in large scale, as silicon is also the main semiconductor material for all electronics; (b) their high manufacturing cost in combination with high costs for installation, accessory components and maintenance, and their low power conversion efficiency (PCE), raise the cost of the produced electricity up to double the typical electricity costs [2]; (c) typical crystalline silicon-based PV panels are rigid, brittle, bulky and heavy. The 2nd generation PVs focus on thin-film technology, including amorphous silicon, CdTe and CIGS PVs, are all expensive alternatives with a long payback time [3].

Hence, alternative materials are being sought to produce PV cells with better processability. Nanostructured carbon and polymer-based electronics are two of the key emerging technologies. Plastic PV cells are light, flexible [4], easy to manufacture at a high volume and low cost, and have the potential to be used in a wide range of applications, such as laptops, to power LEDs, wearable electronics, be incorporated in textiles, and also offer the potential of a large-scale, low-cost production of flexible, film-type solar cells for large

energy conversion and storage systems in buildings (roofs and facades), transport media and space applications. The big challenge is to raise the power conversion efficiency of plastic and organic PVs and cover the full spectrum of light, especially towards the larger wavelengths which are associated with high irradiance values in the solar light spectrum [5].

Plastic PV cells are multilayer assemblies, with an outer transparent conductor, typically ITO, on glass or PET substrates, which have high transparency across the full light spectrum [6]. PEDOT:PSS is the next hole conductor layer, adjacent to ITO, which also has a high transparency of >90% [7] and good conductivity [8]. The active layer of interest in this study is a bulk heterojunction, which comprises a donor/acceptor blend of p- and n-type semiconductors, respectively [9].

Absorption efficiencies of organic PV cells [10–13] are very good in comparison with silicon PV cells for crystalline silicon and even amorphous silicon [14]. Conjugated polymers, used in the active layer and adopted in this study, of different chemical structures, the optical gap and morphology exhibit a maximum value of extinction coefficient of $\kappa = 0.9 \pm 0.1$ [15], where the light absorption coefficient of materials is proportional to the product of the extinction coefficient and frequency of light; this can be to one order of magnitude lower extinction coefficient values for silicon [14]. Typical donor polymers demonstrate light absorbance in the following ranges of the light spectrum: P3HT in 350–650 nm with $\kappa \approx 0.9$ in 470–550 nm; PCDDBT in 300–670 nm with dual peaks and $\kappa \approx 0.9$ at 395 nm and in 500–600 nm; PCPDTBT in 350–880 nm with dual peaks and $\kappa \approx 0.45$ in 390–415 nm and $\kappa \approx 0.9$ in 650–850 nm [15]. The light absorbance of acceptor compounds such as $PC_{61}BM$ and $PC_{70}BM$ peaks in the range of 200 to 400 nm, with $PC_{70}BM$ exhibiting a more than three times higher absorbance than $PC_{61}BM$ [16]. Carbon nanotubes (CNTs) demonstrate a high light absorbance across the full solar spectrum [17,18].

However, despite their higher light absorbance, plastic PVs still suffer from lower external quantum efficiency than silicon PVs, and a major reason for this is poor carrier mobilities. In a conjugated polymer, the mobility of charge carriers depends on the defined timescale, ranging from ultra-high on-chain mobility controlled by the electronic band width of the polymer chain, to retarded mesoscale on-chain motion when encountering defects and to further macroscopic transport via interchain carrier jumps [19]. Attempts to increase carrier injection, for energy conversions similar to those of inorganic solar cells, led to shorter carrier lifetimes due to an increased number of recombinations at the higher charge carrier densities [20]. In a model bilayer heterojunction, the distance between the exciton creation site and the dissociation interface is greater than the diffusion length, resulting in recombination. Mixing the exciton acceptor layer with the donor layer in a nanocomposite type of bulk heterojunction yields shorter distances between the exciton creation site and the exciton dissociation site, which could reduce or eliminate recombination. However, the problem in blended heterojunctions is that the charges will have to hop between many isolated regions, resulting in a decrease in charge mobility [21]. Despite the higher efficiency of recent perovskite PVs, perovskites have low transparency compared to polymer PVs [22], and, for this reason, the present study still focuses on polymer and CNT-polymer nanocomposite PVs which offer the potential for PV window applications.

Several strategies are proposed to increase the charge carrier mobility and applied in this work. Increasing the molecular weight of P3HT by one magnitude improved carrier mobility by three orders of magnitude [23]. Annealing is typically used to coarsen the microstructure and increase the grain size, so the number of intergrain hops is reduced [24,25]. Interpenetrating polymer blends create a large interfacial area for dissociation [26], but the high tortuosity [27,28] lengthens the carrier path to the collector electrode. Charge carriers need a direct pathway to the collecting electrode to maximize their mobility.

CNTs have a good chance to increase charge mobility due to their high aspect ratios [27,29] while they still maintain film transparency if at a low concentration near their percolation threshold [30]. At the percolation threshold, CNTs form a conductive network linked to the corresponding charge extraction outer electrode, although care must be taken

not to form a bridge between the two outer electrodes that could short-circuit the system. Electron/hole selectivity can be achieved through realizing HOMO and LUMO energy bands of the polymers and the work functions of the contacts, where the electron travels to higher energy levels [31,32]. This work investigates further methods to shorten the direct pathway by orienting the CNTs or the polymer grain domains via electrophoresis [33,34] and inkjet printing [35], respectively. Several years ago, it was found in our group that inkjet printing induces the transverse orientation of polymer grains and increases the transverse conductivity of conductive and semiconductive polymer films [35], compared to spin coating with the latter exhibiting a poor transverse conductivity compared to the in-plane conductivity due to the radial orientation of polymer grains during spin coating [8,36]. As a result, the recommendation to be investigated in this study is that the use of inkjet printing or a transverse AC field would benefit the carrier mobility in PV cells rather than spin coating, typically used in the laboratory fabrication of PV cells [37].

2. Proposed PV Cell Designs, Materials and Methods

Figure 1 presents the energy level diagrams of the PV cell concepts assessed in this study. In all cases, the transparent hole collector was the ITO-coated glass (Ossila, Sheffield, UK) coated with a layer of PEDOT:PSS (starting aqueous solution of 1.3% PEDOT:PSS, highly conductive from (Heraeus, Hanau, Germany) and the backplane electron collector was aluminium, thermally evaporated, or aluminium foil (Goodfellow, Huntingdon, UK). Two different bulk heterojunction active layers were created: P3HT:$PC_{61}BM$ in Figure 1a, with poly(3-hexylthiophene-2,5-diyl) (P3HT), regioregular, electronic grade, 99.995% purity (metal basis), average Mn = 17,500 (Sigma-Aldrich, St. Louis, MO, USA) and [6,6]-pentadeuterophenyl C61 butyric acid methyl ester ($PC_{61}BM$) of 99.5% purity (Sigma-Aldrich, St. Louis, MO, USA) which represents a distribution of quantum dots of C61 attached on the polymer chain. PCDTBT:$PC_{70}BM$ in Figure 1b with PCDTBT with MW = 42,200 (Ossila, Sheffield, UK) and $PC_{70}BM$ of 99% purity (Ossila, Sheffield, UK). Multiwall CNTs were Elicarb® multiwall carbon nanotubes of 10–30 nm diameter and microns length (Thomas Swan, Consett, UK) and were deposited on the aluminium foil backplane. Figure 1c shows that the HOMO–LUMO gap of MWCNTs was very small, but could act as acceptor when combined with a donor polymer, where even PEDOT:PSS exhibited a small HOMO–LUMO gap of 1.5 eV.

All solution preparation and cell fabrication took place mostly in an argon-filled glovebox (H_2O < 0.5 ppm; O_2 < 0.5 ppm). The donor and acceptor polymers were dissolved in 1,2-dichlorobenzene at a concentration of 7 mg mL^{-1}. The mixture was stirred, under the inert environment, using a magnetic stirrer and left overnight for approximately 16 h. A pre-patterned ITO-glass substrate was used (Ossila, UK) with six cells of 1.5 mm × 4 mm each and attached electrical connection legs (Figure 2), so 6 PV cells were fabricated and tested for each type of PV cell investigated in this study. Two alternative methods were used to deposit all the solutions: spin coating at 5000 rpm or inkjet printing from a 100 µm nozzle [35], where the substrate was fixed on a 2D moving platform under the stationary inkjet nozzle [35]. The layer deposition followed the sequence: PEDOT:PSS on ITO; polymer heterojunction blend on PEDOT:PSS; all solutions were dried on a hot plate at 80 °C for 10 min; aluminium vaporization; outer glass slide sandwiching the PV assembly for ease of handling. A third method was also applied, where the passive PEDOT:PSS layer was spin coated and the active bulk heterojunction blend was inkjet printed. In the case of also adding MWCNTs, the following procedure was performed: MWCNTs in NMP solution at a concentration of 0.14% w/v were deposited on aluminium foil using two alternative methods—casting from a 10 µL pipette or electrophoretic deposition to induce MWCNT orientation [34]; the polymer heterojunction blend was deposited on the MWCNT layer and, also, as a thin layer on the PEDOT:PSS/ITO-PET, and the two sides were quickly brought into contact before the heterojunction was completely dry. All cells were annealed in dichlorobenzene vapor for 1 h at 80 °C. In the case of MWCNT additive, the cell was annealed under a transverse AC field to maintain and reinforce the MWCNT orientation

aiming at obtaining the architecture depicted in Figure 3 which focuses on short charge carrier paths. The common solvents for both donor and acceptor polymers facilitated the polymer PV recycling route via dissolution processes [38–41]. The MWCNT layers (electrophoretically deposited or cast) were examined under a JEOL scanning electron microscope (SEM).

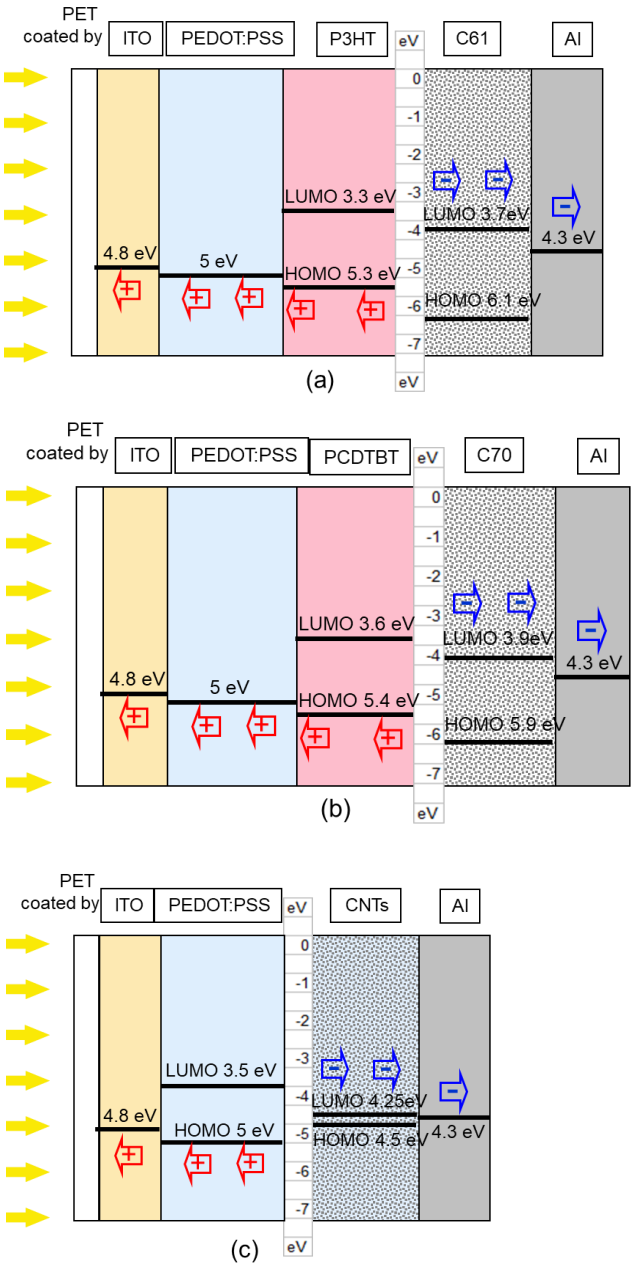

Figure 1. Energy level diagrams of different PV cell designs and flow of the positive and negative charge carriers. (**a**) typical ITO/PEDOT:PSS/P3HT/C_{61}/Al, (**b**) ITO/PEDOT:PSS/PCDTBT/C_{70}/Al, (**c**) ITO/PEDOT:PSS/CNT/Al.

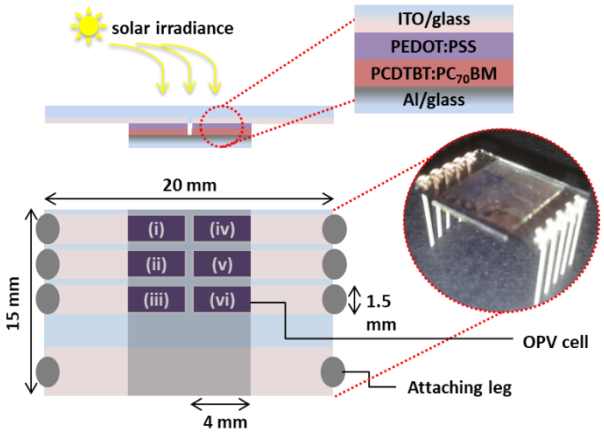

Figure 2. Patterned substrate pack (Ossila, UK) used for the fabrication of PV cells as shown in the example above.

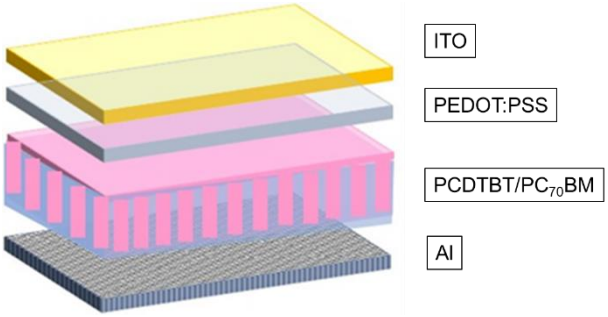

Figure 3. Diagram of PV concept with optimized nanostructure architecture to minimize the pathway of the charge carriers.

Each fabricated cell was characterized in the light using a solar simulator at 1 sun, AM 1.5 G, i.e., irradiance of 100 mW cm^{-2}. *I–V* measurements under light conditions were carried out using a Gamry Interface 1010E device, changing the voltage, V, at a constant rate and measuring the current density, J, to produce a *J–V* graph. Important parameters from the graph were the open-circuit voltage, V_{oc}, the closed-circuit current density, J_{sc}, the maximum power density, P_{max}, and the fill factor, FF:

$$FF = \frac{P_{max}}{J_{sc} V_{oc}} \quad (1)$$

The overall power conversion efficiency (PCE) was calculated as a function of the inputted light power, P_{in} (P_{in} = 100 mW cm^{-2} in our study), according to the relation:

$$PCE = \frac{P_{max}}{P_{in}} \quad (2)$$

3. Results

Table 1 displays the key performance parameters for all tested cells as derived from their *J–V* plots. Figures 4 and 5 present the *J–V* plot for the PV cells ITO/PEDOT:PSS/P3HT/C_{61}/Al and ITO/PEDOT:PSS/PCDTBT/C_{70}/Al, respectively, fabricated by spin coating or inkjet printing. In general, the PCDTBT/C_{70} bulk heterojunction exhibited a better PCE due to both its higher values of V_{oc} and J_{sc}. This may be due to the larger amount of integrated light absorption by PCDTBT across the whole UV–Vis–IR spectrum compared to the single absorption peak of P3HT around 470–550 nm [15].

Table 1. Key performance parameters of the PV cells investigated in this paper: theoretical V_{oc} according to Equation (3) and values of all parameters from the experimental testing of PV cells; each experimental value is the average of six tested cells, accompanied by the standard error.

PV	*Th.* V_{oc} (V)	V_{oc} (V)	R_s (W cm^2)	R_{sh} (W cm^2)	J_{sc} (mA cm^{-2})	FF	P_{max} (mW cm^{-2})	PCE (%)
ITO/PEDOT:PSS/P3HT/C_{61}/Al								
Spin coated–Spin coated	1.3	0.7 ± 0.1	5.0	8008	7.0 ± 0.2	0.66 ± 0.1	3.2 ± 0.3	3.2 ± 0.3
Inkjet printed–Inkjet printed		0.63 ± 0.1	10.5	267	7.4 ± 0.3	0.54 ± 0.1	2.5 ± 0.5	2.5 ± 0.5
Spin coated–Inkjet printed		0.7 ± 0.1	10.0	801	7.0 ± 0.2	0.67 ± 0.1	3.2 ± 0.3	3.2 ± 0.3
ITO/PEDOT:PSS/PCDTBT/C_{70}/Al								
Spin coated–Spin coated	1.25	0.91 ± 0.2	8.3	811	12.8 ± 0.2	0.65 ± 0.1	7.6 ± 0.4	7.6 ± 0.4
Inkjet printed–Inkjet printed		0.89 ± 0.2	8.0	200	13.7 ± 0.3	0.54 ± 0.1	6.6 ± 0.5	6.6 ± 0.5
Spin coated–Inkjet printed		0.91 ± 0.2	7.5	1334	13.7 ± 0.3	0.69 ± 0.1	8.6 ± 0.5	8.6 ± 0.5
ITO/PEDOT:PSS/CNT/Al								
Cast–Cast	0.45	0.49 ± 0.2	4	80	0.3 ± 0.2	0.4	0.06 ± 0.1	0.06 ± 0.1
Cast–Electrophoresis		0			0		0	0
ITO/PEDOT:PSS/PCDTBT/C_{70}/CNT/Al	1.25							
Cast		1.01 ± 0.1	57	801	14.7 ± 0.5	0.71 ± 0.3	11.1 ± 0.6	11.1 ± 0.6

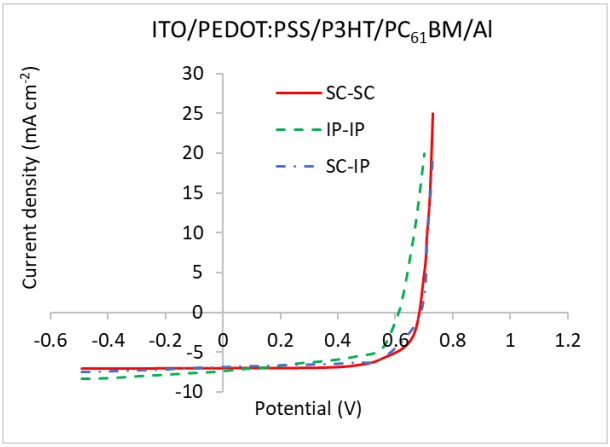

Figure 4. J–V plots for the ITO/PEDOT:PSS/P3HT/PC_{61}BM/Al PV cells fabricated via spin coating (SC) or inkjet printing (IP) of all layers or spin coating of PEDOT:PSS and inkjet printing of the P3HT/PC_{61}BM solution (SC-IP).

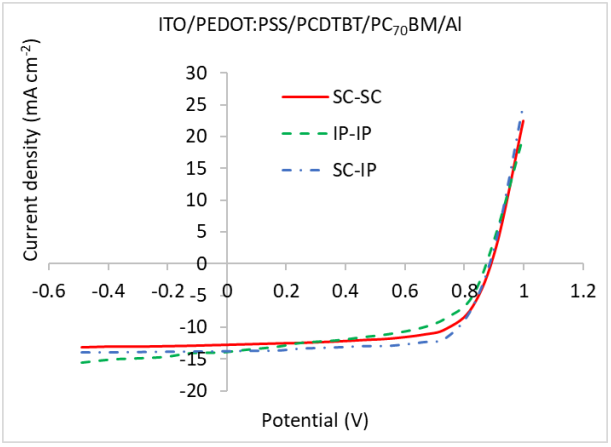

Figure 5. J–V plots for the ITO/PEDOT:PSS/PCDTBT/PC_{70}BM/Al PV cells fabricated via spin coating (SC) or inkjet printing (IP) of all layers or spin coating of PEDOT:PSS and inkjet printing of the PCDTBT/PC_{70}BM solution (SC-IP).

Apart from the key performance parameters defined in Section 2, the in-series areal resistance, R_s, and the shunt areal resistance, R_{sh}, were also calculated from the *J*–*V* plots as the inverse of the slope at $J = 0$ and $V = 0$, respectively, and are presented in Table 1. In order to maximize the fill factor, FF, close to 1, it was desirable that $R_s = 0$ and $R_{sh} = \infty$.

In general, it was observed that the inkjet printing of both the passive layer (PEDOT:PSS) and the active layer (bulk heterojunction blend) was not beneficial: although it increased the J_{sc} value, it decreased both the FF and PCE values, due to a decrease in the shunt resistance. It is believed that the reason for the decrease in R_{sh} values of the PVs with the inkjet-printed passive layer was due to discontinuities caused by the deposited droplet shape [36], which created troughs and valleys at the PEDOT:PSS surface and possible voids upon the subsequent printing of the active layer. In contrast, spin coating produces thin smooth layers of low roughness [36]. Hence, a third deposition procedure comprised spin coating of the passive PEDOT:PSS layer and inkjet printing of the active bulk heterojunction blend layer. This method seemed to produce the best PVs, especially of the ITO/PEDOT:PSS/PCDTBT/C_{70}/Al-type, with an increased shunt resistance, decreased in-series resistance and high J_{sc}, overall resulting in the best FF and PCE values.

Figure 6a depicts that, when electrophoretically deposited on the aluminium foil, MWCNTs formed tall bumps several microns high. This would easily short-circuit the cell, with V_{oc} = 0, as shown in Table 1 for the corresponding ITO/PEDOT:PSS/CNT/Al cell. For this reason, we tried to cast a thick layer of the active heterojunction blend on top of the MWCNTs, but this produced a large in-series resistance and J_{sc} = 0. Casting was preferred to spin coating or inkjet printing due to the thick layer of the MWCNT layer (tall MWCNT bumps created by electrophoresis) in Figure 6a that needed to be impregnated by an equally thick adjacent polymer layer. Due to the resulting J_{sc} = 0 for the oriented MWCNTs, a dilute solution of MWCNTs was cast on the aluminium foil producing a much thinner layer of homogeneously distributed and well dispersed MWCNTs as depicted in Figure 6b. The cast ITO/PEDOT:PSS/CNT/Al cell exhibited some PV properties, but it was clear that the limited semiconducting behaviour of both PEDOT:PSS and MWCNTs (Figure 1c) reduced the PV performance.

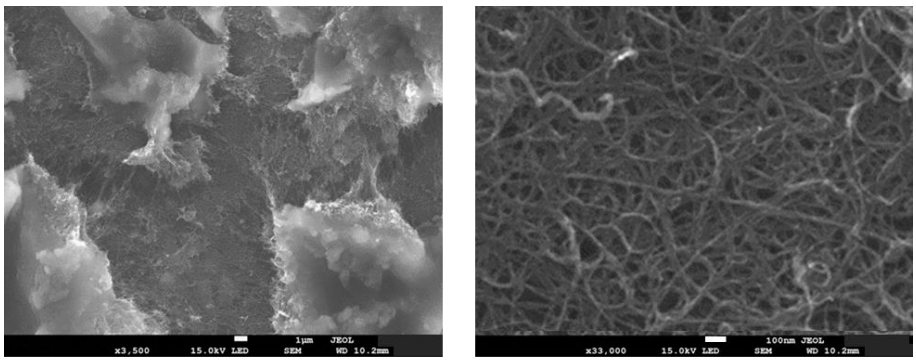

Figure 6. SEM micrographs of PCDTBT/PC_{70}BM/MWCNT layer with cast PCDTBT/PC_{70}BM on top of the MWCNT layer, where the MWCNTs were deposited (**a**) by electrophoresis and (**b**) by casting of the MWCNT solution.

Finally, a layered nanostructure was formed with the best so far performance active layer PCDTBT/PC_{70}BM and a CNT network cast on the aluminium foil; subsequently, the PCDTBT/PC_{70}BM layer was cast on top of the CNT network. At the same time, an ITO-glass slide was prepared with spin coated PEDOT:PSS and a thin spin coated layer of PCDTBT/PC_{70}BM. The two sides were then quickly pressed into contact before the heterojunction was completely dry. The cell assembly was finally exposed in dichlorobenzene vapor for 1 h at 80 °C and under the presence of a transverse AC field, so the polymer materials were annealed and formed elongated grains oriented transversely to the cell under the AC field [33,35]. Figure 7 presents the J–V plot for this PV cell and Table 1 demonstrates that this was the best performing PV cell in this study, with V_{oc} = 1.01 V and PCE = 11.1%.

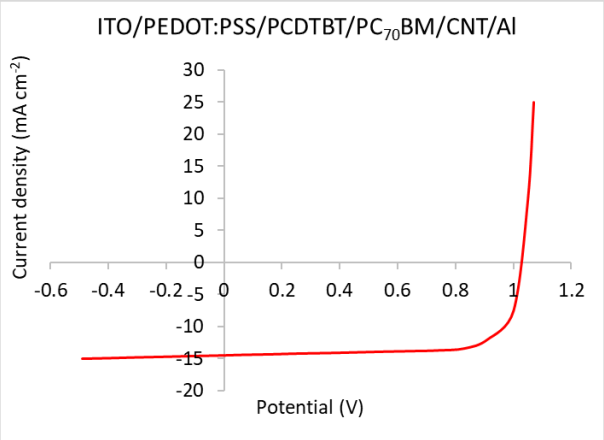

Figure 7. J–V plot for the ITO/PEDOT:PSS/PCDTBT/PC_{70}BM/CNT/Al PV cell, where all layers were fabricated via casting, accompanied by cell annealing in dichlorobenzene vapor for 1 h at 80 °C and under the presence of transverse AC field.

4. Discussion

The first objective in the selection of suitable active polymers was to maximize the absorption of light, especially in the IR and UV areas of the spectrum. Figure 1c shows that PEDOT:PSS had a small energy gap of 1.5 eV which meant that PEDOT:PSS was highly absorbent of IR light that comprised 52% of the sunlight energy, whereas it was transparent to the Vis part of the solar spectrum, making PEDOT:PSS an excellent donor polymer for PV windows. The next best donor amongst the investigated polymers would be PCDTBT with an energy gap of 1.8 eV, which in fact also had a high absorbance in UV light and, overall, absorbed a greater amount of energy across the UV–Vis–IR spectrum compared to P3HT, which exhibited a single absorption peak at 470–550 nm [15]. This was a major reason for the better performance of the PCDTBT/PCBM PVs against the P3HT/PCBM PVs in this study.

The second objective was to maximize V_{oc}, which could be estimated from the following relation according to the Scharber model for the conjugated polymer–PCBM PV cell [32,42]:

$$V_{oc} = \frac{1}{e}\left[E_{HOMO}^{Donor} - E_{LUMO}^{Acceptor}\right] - 0.3V \quad (3)$$

Table 1 displays a very low value for the theoretical V_{oc} of the ITO/PEDOT:PSS/CNT/Al cell which is confirmed by the experimental value. Scharber et al. [32] also constructed a contour map of predicted PCE values for conjugated polymer–PCBM PV cells based on the energy gap and the LUMO level of the donor. According to this contour map, the PCE values were estimated as PCE = 6.5% and 4.5% for the P3HT/PCBM and the PCDTBT/PCBM bulk heterojunctions, respectively, which was attributed to the higher estimated V_{oc} value for the P3HT/PCBM cell (using Equation (3)), as displayed in Table 1.

However, the experimental V_{oc} data were lower than the theoretical values in Table 1, especially for the P3HT/C_{61} bulk heterojunction. In general, there are more factors affecting V_{oc}, apart from the energy difference between the donor HOMO and the acceptor LUMO levels [43]. These include a logarithmic dependence on the J_{sc} value, where the P3HT/C_{61} cells seem to exhibit about half the J_{sc} value of the PCDTBT/C_{70} cells and on the density of states at the conduction band edge of the donor polymer and the fullerene acceptor. In general, a high crystallinity of the donor polymer encourages upward shifts in its HOMO level, whereas small variations in the LUMO level of the acceptor fullerene influence the V_{oc} value. Hence, the PCDTBT/C_{70} cells were superior to the P3HT/C_{61} cells in this study, attributed to both the greater amount of absorbed light energy and the higher J_{sc} values of the former bulk heterojunction.

Much effort was concentrated on developing the layer deposition methodology for the cells containing MWCNTs, as it was thought that an MWCNT network would aid rapid electron extraction by the outer current collector. Although it was initially thought that the electrophoretic deposition of MWCNTs would induce orientation which would facilitate and accelerate electron transport to the aluminium current collector, the deposited MWCNT bumps were very tall, as seen in Figure 6a, which either short-circuited the cell (V_{oc} = 0) or, when casting a very thick active polymer layer over the MWCNTs, increased the in-series resistance and minimized J_{sc}. Therefore, in the end, the casting of MWCNTs on the aluminium foil provided a continuous homogeneous conducting network in imminent contact with the bulk heterojunction as the latter was cast on the MWCNTs to embed their network in the heterojunction. The solvothermal annealing of the polymers under the transverse AC field induced polymer grain coarsening, elongation and transverse orientation, resembling the paradigm presented in Figure 3. Such oriented nanostructures shorten the path length of the charge carriers reducing the number of charge recombinations. As a result, this PV exhibited the highest J_{sc} of all cells (Table 1 and Figure 7), which contributed to the elevation of *Voc* to 1.01 V for the PCDTBT/C_{70} heterojunction, closer to its initially estimated value of 1.25 V (Figure 1b), resulting in the highest measured PCE value in this study of 11.1%.

The next question was whether the scaling up of these cells might be detrimental to their performance, as it has been reported [44] that increasing the PV cell area decreased the J_{sc} and FF values, but increases the V_{oc}. The most important issue was that larger PV areas suffered from reproducibility problems as there was a larger chance for defects [44]. As a result, large-scale fabrication roll-to-roll methods are critical in maintaining PV performance of scaled-up PV films. Examples of suitable roll-to-roll techniques include slot die deposition, which could be equivalent to casting, printing techniques, and curtain spraying which could be equivalent to large-scale inkjet printing [45]. Such methods could be set on flat beds and easily combined with a localized transverse AC field.

5. Conclusions

A polymer blend and nanocomposite nanostructures were investigated in this study in terms of both materials and optimized architectures for polymer PVs. It was found that PCDTBT/PC_{70}BM had a better performance than P3HT/PC_{61}BM due to the greater light absorption across the full spectrum and the high J_{sc} of the former, which also led to a higher V_{oc}. A transverse orientation of the bulk heterojunction polymers via inkjet printing or transverse AC field during annealing further increased the J_{sc} value, as it reduced the path length of charge carriers and the chances of charge recombination. However, inkjet printing and electrophoretic deposition of the conductive layers of PEDOT:PSS or MWCNTs, respectively, lowered the PV performance, as it created roughness at the surface of the conductive layer(s) and short circuiting. For this reason, a homogeneous thin layer of MWCNTs was deposited by casting on the aluminium current collector to reinforce the fast transport and extraction of electrons. Overall, the ITO/PEDOT:PSS/PCDTBT/PC_{70}BM/CNT/Al PV cell, fabricated with the optimized procedure, delivered the best performance at *PCE* = 11.1%, with V_{oc} = 1.01 V.

Author Contributions: Conceptualization, C.L.; methodology, C.L., F.M., T.A., G.N. and I.Z.; formal analysis, C.L. and T.A.; investigation, C.L., F.M., T.A., G.N. and I.Z.; resources, C.L.; data curation, C.L.; writing—original draft preparation, G.N., I.Z., T.A., F.M. and C.L.; writing—review and editing, C.L.; visualization, F.M. and C.L.; supervision, C.L.; project administration, C.L.; funding acquisition, C.L. All authors have read and agreed to the published version of the manuscript.

Funding: This research was funded by IeMRC, UK which was in turn funded by EPSRC, UK.

Conflicts of Interest: The authors declare no conflict of interest.

References

1. Battaglia, C.; Cuevas, A.; De Wolf, S. High-efficiency crystalline silicon solar cells: Status and perspectives. *Energy Environ. Sci.* **2016**, *9*, 1552–1576. [CrossRef]
2. IRENA. *Renewable Power Generation Costs in 2019*; International Renewable Energy Agency: Abu Dhabi, United Arab Emirates, 2020; pp. 18–45, 60–73, 120–129.
3. Spooner, E. Organic Photovoltaics vs. 2nd-Generation Solar Cell Technologies. Available online: https://www.ossila.com/pages/organic-photovoltaics-vs-2nd-gen-solar-cell-tech (accessed on 19 August 2021).
4. Lungenschmied, C.; Dennler, G.; Neugebauer, H.; Sariciftci, S.N.; Glatthaar, M.; Meyer, T.; Meyer, A. Flexible, long-lived, large-area, organic solar cells. *Sol. Energy Mater. Sol. Cells* **2007**, *91*, 379–384. [CrossRef]
5. Subhan, F.E.; Khan, A.D.; Hilal, F.E.; Khan, A.D.; Khan, S.D.; Ullah, R.; Imran, M.; Noman, M. Efficient broadband light absorption in thin-film a-Si solar cell based on double sided hybrid bi-metallic nanogratings. *RSC Adv.* **2020**, *10*, 11836–11842. [CrossRef]
6. Bok, S.; Seok, H.-J.; Kim, Y.A.; Park, J.-H.; Kim, J.; Kang, J.; Kim, H.-K.; Lim, B. Transparent molecular adhesive enabling mechanically stable ITO thin films. *ACS Appl. Mater. Interfaces* **2021**, *13*, 3463–3470. [CrossRef]
7. Singh, V.; Kumar, T. Study of modified PEDOT:PSS for tuning the optical properties of its conductive thin films. *J. Sci. Adv. Mater. Devices* **2019**, *4*, 538–543. [CrossRef]
8. P Wilson, P.; Lekakou, C.; Watts, J.F. A comparative assessment of surface microstructure and electrical conductivity dependence on co-solvent addition in spin coated and inkjet printed poly (3, 4 ethylenedioxythiophene):polystyrene sulphonate (PEDOT:PSS). *Org. Electron.* **2012**, *13*, 409–418. [CrossRef]
9. Li, X.; Li, P.; Wu, Z.; Luo, D.; Yu, H.-Y.; Lu, Z.-H. Review and perspective of materials for flexible solar cells. *Mater. Rep. Energy* **2021**, *1*, 100001.
10. Vanlaeke, P.; Vanhoyland, G.; Aernouts, T.; Cheyns, D.; Deibel, C.; Manca, J.; Heremans, P.; Poortmans, J. Polythiophene based bulk heterojunction solar cells: Morphology and its implications. *Thin Solid Film.* **2006**, *511–512*, 358–361. [CrossRef]
11. Luzzati, S.; Basso, M.; Catellani, M.; Brabec, C.J.; Gebeyehu, D.; Sariciftci, N.S. Photo-induced electron transfer from a dithieno thiophene-based polymer to TiO_2. *Thin Solid Film.* **2002**, *403–404*, 52–56. [CrossRef]
12. Hoppe, H.; Sariciftci, N.S. Morphology of polymer/fullerene bulk heterojunction solar cells. *J. Mater. Chem.* **2006**, *16*, 45–61. [CrossRef]
13. Kim, J.Y.; Kim, S.H.; Lee, H.-H.; Lee, K.; Ma, W.; Gong, X.; Heeger, A.J. New architecture for high-efficiency polymer photovoltaic cells using solution-based titanium oxide as an optical spacer. *Adv. Mater.* **2006**, *18*, 572–576. [CrossRef]
14. Kang, H. Crystalline silicon vs. amorphous silicon: The significance of structural differences in photovoltaic applications. *IOP Conf. Ser. Earth Environ. Sci.* **2021**, *726*, 012001. [CrossRef]
15. Vezie, M.S.; Few, S.; Meager, I.; Pieridou, G.; Dörling, B.; Ashraf, R.S.; Goñi, A.R.; Bronstein, H.; McCulloch, I.; Hayes, S.C.; et al. Exploring the origin of high optical absorption in conjugated polymers. *Nat. Mater.* **2016**, *15*, 746–753. [CrossRef]
16. Hou, J.; Guo, X. Active layer materials for organic solar cells. In *Organic Solar Cells*; from Green Energy and Technology Book Series; Choy, W.C.H., Ed.; Springer: London, UK, 2013; pp. 17–42.
17. Fagan, J.A.; Simpson, J.R.; Bauer, B.J.; De Paoli Lacerda, S.H.; Becker, M.L.; Chun, J.; Migler, K.B.; Hight Walker, A.R.; Hobbie, E.K. Length-dependent optical effects in single-wall carbon nanotubes. *J. Am. Chem. Soc.* **2007**, *29*, 10607–10612. [CrossRef]
18. Bunes, B.R.; Xu, M.; Zhang, Y.; Gross, D.E.; Saha, A.; Jacobs, D.L.; Yang, X.; Moore, J.S.; Zang, L. Photodoping and enhanced visible light absorption in single-walled carbon nanotubes functionalized with a wide band gap oligomer. *Adv. Mater.* **2015**, *27*, 162–167. [CrossRef]
19. Laquai, F.; Wegner, G.; Bässler, H. What determines the mobility of charge carriers in conjugated polymers? *Philos. Trans. R. Soc. A Math. Phys. Eng. Sci.* **2007**, *365*, 1473–1487. [CrossRef] [PubMed]
20. Juska, G.; Alauskas, K.; Sliauzys, G.; Pivrikas, A.; Mozer, A.J.; Sariciftci, N.S. Double injection as a technique to study charge carrier transport and recombination in bulk-heterojunction solar cells. *Appl. Phys. Lett.* **2005**, *87*, 222110. [CrossRef]
21. Kroon, J.M.; Bakker, N.J.; Smit, H.J.P.; Liska, P.; Thampi, K.R.; Wang, P.; Zakeeruddin, S.M.; Gratzel, M.; Hinsch, A.; Hore, S.; et al. Nanocrystalline dye-sensitized solar cells having maximum performance. *Prog. Photovolt. Res Appl.* **2007**, *15*, 1–18. [CrossRef]
22. Rahmany, S.; Etgar, L. Semitransparent perovskite solar cells. *ACS Energy Lett.* **2020**, *5*, 1519–1531. [CrossRef]
23. Salleo, A. Charge transport in polymeric transistors. *Mater. Today* **2007**, *10*, 38–45. [CrossRef]
24. Liu, F.; Gu, Y.; Jung, J.W.; Jo, W.H.; Russell, T.P. On the morphology of polymer-based photovoltaics. *J. Polym. Sci. Part B Polym. Phys.* **2012**, *50*, 1018–1044. [CrossRef]
25. Hamdeh, U.H.; Nelson, R.D.; Ryan, B.J.; Bhattacharjee, U.; Petrich, J.W.; Panthani, M.G. Solution-processed BiI3 thin films for photovoltaic applications: Improved carrier collection via solvent annealing. *Chem. Mater.* **2016**, *28*, 6567–6574. [CrossRef]
26. Xie, L.; Song, W.; Ge, J.; Tang, B.; Zhang, X.; Wu, T.; Ge, Z. Recent progress of organic photovoltaics for indoor energy harvesting. *Nano Energy* **2021**, *82*, 105770. [CrossRef]
27. Vermisoglou, E.C.; Giannakopoulou, T.; Romanos, G.E.; Boukos, N.; Giannouri, M.; Lei, C.; Lekakou, C.; Trapalis, C. Non-activated high surface area expanded graphite oxide for supercapacitors. *Appl. Surf. Sci.* **2015**, *358*, 110–121. [CrossRef]
28. Lei, C.; Lekakou, C. Activated carbon–carbon nanotube nanocomposite coatings for supercapacitor applications. *Surf. Coat. Technol.* **2013**, *232*, 326–330. [CrossRef]
29. Wijewardane, S. Potential applicability of CNT and CNT/composites to implement ASEC concept: A review article. *Sol. Energy* **2009**, *83*, 1379–1389. [CrossRef]

30. Rebord, G.; Hansrisuk, N.; Lindsay, B.; Lekakou, C.; Reed, G.T.; Watts, J.F. Electrofunctional polymer nanocomposites. In Proceedings of the 2008 2nd Electronics System-Integration Technology Conference, Florence, Italy, 1–4 September 2016; IEEE NY: Greenwich, UK, 2008; pp. 1401–1406.
31. Derouiche, H.; Djara, V. Impact of the energy difference in LUMO and HOMO of the bulk heterojunctions components on the efficiency of organic solar cells. *Sol. Energy Mater. Sol. Cells* **2007**, *91*, 1163–1167. [CrossRef]
32. Scharber, M.C.; Muhlbacher, D.; Koppe, M.; Denk, P.; Waldauf, C.; Heeger, A.J.; Braber, C.J. Design rules for donors in bulk-heterojunction solar cells—Towards 10% energy-conversion efficiency. *Adv. Mater.* **2006**, *18*, 789–794. [CrossRef]
33. Murugesh, A.K.; Uthayanan, A.; Lekakou, C. Electrophoresis and orientation of multiple wall carbon nanotubes in polymer solution. *Appl. Phys. A* **2010**, *100*, 135–144. [CrossRef]
34. Markoulidis, F.; Lei, C.; Lekakou, C. Fabrication of high-performance supercapacitors based on transversely oriented carbon nanotubes. *Appl. Phys. A* **2013**, *111*, 227–236. [CrossRef]
35. Wilson, P.; Lei, C.; Lekakou, C.; JF Watts, J.F. Transverse charge transport in inkjet printed poly (3, 4-ethylenedioxythiophene) polystyrene sulfonate (PEDOT: PSS). *Org. Electron.* **2014**, *15*, 2043–2051. [CrossRef]
36. Wilson, P.; Lekakou, C.; JF Watts, J.F. In-plane conduction characterisation and charge transport model of DMSO co-doped, inkjet printed Poly (3, 4-ethylenedioxythiophene): Polystyrene sulfonate (PEDOT: PSS). *Org. Electron.* **2013**, *14*, 3277–3285. [CrossRef]
37. Wantana, K.; Aniwat, P.; Bunlue, S.; Alongkot, T.; Anusit, K.; Pisist, K. Study of thin film coating technique parameters for low cost organic solar cells fabrication. *Mater. Today Proc.* **2017**, *4*, 6626–6632. [CrossRef]
38. Chowdhury, S.; Rahman, K.S.; Chowdhury, T.; Nuthammachot, N.; Techato, K.; Sieh, A.; Tiong, S.K.; Sopian, K.; Amin, N. An overview of solar photovoltaic panels' end-of-life material recycling. *Energy Strategy Rev.* **2020**, *27*, 100431. [CrossRef]
39. Vermisoglou, E.C.; Giannouri, M.; Todorova, N.; Giannakopoulou, T.; Lekakou, C.; Trapalis, C. Recycling of typical supercapacitor materials. *Waste Manag. Res.* **2016**, *34*, 337–344. [CrossRef]
40. Kampouris, E.M.; Papaspyrides, C.D.; Lekakou, C.N. A model recovery process for scrap polystyrene foam by means of solvent systems. *Conserv. Recycl.* **1987**, *10*, 315–319. [CrossRef]
41. Kampouris, E.M.; Papaspyrides, C.D.; Lekakou, C.N. A model process for the solvent recycling of polystyrene. *Polym. Eng. Sci.* **1988**, *28*, 534–537. [CrossRef]
42. Yeboah, D.; Singh, J. Study of the contributions of donor and acceptor photoexcitations to open circuit voltage in bulk heterojunction organic solar cells. *Electronics* **2017**, *6*, 75. [CrossRef]
43. Elumalai, N.K.; Uddin, A. Open circuit voltage of organic solar cells: An in-depth review. *Energy Environ. Sci.* **2016**, *9*, 391–410. [CrossRef]
44. Rozanski, L.J.; Smith, C.T.G.; Gandhi, K.K.; Beliatis, M.J.; Dabera, G.D.M.R.; Jayawardena, K.D.G.I.; Adikaari, A.A.D.T.; Kearney, M.J.; Silva, S.R.P. A critical look at organic photovoltaic fabrication methodology: Defining performance enhancement parameters relative to active area. *Sol. Energy Mater. Sol. Cells* **2014**, *130*, 513–520. [CrossRef]
45. Sampaio, P.C.V.; González, M.O.A.; de Oliveira Ferreira, P.; da Cunha Jácome Vidal, P.; Pereira, J.P.P.; Ferreira, H.R.; Oprime, P.C. Overview of printing and coating techniques in the production of organic photovoltaic cells. *Int. J. Energy Res.* **2020**, *44*, 9912–9931. [CrossRef]